

# PROGRESS REPORT ON METHODS OF LOCAL HELIOSEISMOLOGY

L. Gizon<sup>1</sup>, J. Jackiewicz<sup>1</sup>, A. C. Birch<sup>\*2</sup>, and T. L. Duvall Jr.<sup>3</sup>

<sup>1</sup>Max-Planck-Institut für Sonnensystemforschung, 37191 Katlenburg-Lindau, Germany

<sup>2</sup>Colorado Research Associates, NorthWest Research Associates Inc., Boulder, CO 80301, USA

<sup>3</sup>Laboratory for Solar and Space Physics, NASA Goddard Space Flight Center, Greenbelt, MD 20771, USA

## Abstract

We discuss various methods of interpretation of solar oscillations in the context of time-distance and ring-diagram analyses. In particular, we investigate the effect of flows on travel times and ring parameters and we provide a test of the Born approximation to compute the effect of small magnetic perturbations. We also present direct observations of travel-time shifts due to localised magnetic features.

Key words: Local helioseismology, solar oscillations, Sun: rotation, convection, magnetic fields.

## 1. INTRODUCTION

This paper is a collection of recent results and notes that we think are important steps toward a proper quantitative interpretation of local helioseismology data. We consider two methods of local helioseismology: time-distance and ring-diagram analyses (see Gizon & Birch, 2005, and references therein).

In local helioseismology, the governing equations of solar oscillations are often written in plane-parallel geometry. This approximation is typically valid over a small fraction of the solar disk for horizontal wavelengths that are much smaller than the solar radius. The signal used in helioseismology is the line-of-sight component of the wave velocity:

$$\phi(\mathbf{x}, t) = \text{PSF}(\mathbf{x}) \star [\boldsymbol{\ell}(\mathbf{x}) \cdot \partial_t \boldsymbol{\xi}(\mathbf{x}, z_0, t)], \quad (1)$$

where  $\mathbf{x}$  is a horizontal position vector on the solar surface (defined by height  $z_0$ ),  $t$  is time,  $\boldsymbol{\ell}$  is a unit vector pointing in the direction of the observer, and  $\boldsymbol{\xi}$  is the wave displacement vector. Convolution by the point spread function of the telescope, denoted by PSF, is included. It is customary to consider the data cube  $\phi(\mathbf{x}, t)$  in a reference frame which is co-rotating with the Sun to remove the main component of rotation. Note that observers sometimes use the oscillation signal measured in intensity, although the line-of-sight velocity is most common.

In time-distance helioseismology, the oscillation signal is filtered in 3D Fourier space to obtain

$$\psi(\mathbf{k}, \omega) = F_i(\mathbf{k}, \omega) \phi(\mathbf{k}, \omega), \quad (2)$$

where  $\mathbf{k}$  is the horizontal wave vector,  $\omega$  is the angular frequency, and  $F_i$  is a filter chosen by the observer to remove granulation noise and to select parts of the propagation diagram. A standard procedure is to use phase-speed filters (Duvall et al., 1997). This choice of filter is based on the fact that acoustic waves with the same phase speed  $\omega/k$  travel the same horizontal distance.

In ring-diagram analysis (e.g. Haber et al., 2004), the signal is apodized by a function  $A$  that depends on the distance from a target location  $\mathbf{x}_0$ :

$$\Psi(\mathbf{x}, t; \mathbf{x}_0) = A(\mathbf{x}; \mathbf{x}_0) \phi(\mathbf{x}, t). \quad (3)$$

---

\*Supported by NASA contract NNH04CC05C

Typically,  $A$  is a 2D Gaussian-like function with a full-width of  $15^\circ$ . The apodized signal  $\Psi$  is then Fourier transformed to give the local power spectrum

$$P(\mathbf{k}, \omega; \mathbf{x}_0) = \left| \int A(\mathbf{k} - \mathbf{k}'; \mathbf{x}_0) \phi(\mathbf{k}', \omega) d^2 \mathbf{k}' \right|^2. \quad (4)$$

In Sections 2 and 3 we describe simple methods to extract measurements of travel times from  $\psi$  (for time-distance helioseismology) and ring parameters from  $P$  (for ring-diagram analysis). Section 4 is a discussion of the stochastic noise associated with these measurements. After a short discussion of the first Born approximation (Sect. 5), we derive kernel functions that give the linear sensitivity of travel times (Sect. 6) and ring parameters (Sect. 7) to a steady flow in the Sun. In Section 8 we study the effect of a weak magnetic field on the wavefield. In Section 9, observations of travel-time shifts introduced by small network magnetic features are presented.

## 2. TRAVEL TIMES

In time-distance helioseismology, we compute the temporal cross-covariance function between the line-of-sight velocities at two surface locations  $\mathbf{x}_1$  and  $\mathbf{x}_2$ :

$$C(\mathbf{x}_1 | \mathbf{x}_2, t) = \frac{1}{T - |t|} \int \psi(\mathbf{x}_1, t') \psi(\mathbf{x}_2, t' + t) dt', \quad (5)$$

where  $T$  is the duration of the observation and  $\psi$  is the observed signal. Multiplication by the temporal window function (equal to unity in the interval  $[-T/2, T/2]$  and zero outside) is included in the definition of  $\psi$ . The positive time lags ( $t > 0$ ) give information about waves propagating from  $\mathbf{x}_1$  to  $\mathbf{x}_2$ , and the negative time lags ( $t < 0$ ) give information about waves propagating in the opposite direction. In most applications, the wave travel times are measured from the first-skip correlations.

Two methods are used to measure travel times. The first method consists of fitting a Gaussian wavelet to each first-skip branch of the cross-covariance. For example, the positive-time part of the cross-covariance is fitted with a function of the form

$$A \exp[-\gamma^2(t - t_g)^2] \cos[\omega_0(t - \tau_+)], \quad (6)$$

where all parameters are free. The time  $\tau_+$  is called the phase travel time. Similarly a phase travel time  $\tau_-$  is measured by fitting a wavelet to the negative-time part of the cross-covariance. The travel-time differences  $\tau_{\text{diff}}(\mathbf{x}_1 | \mathbf{x}_2) = \tau_+ - \tau_-$  are mostly sensitive to flows, while the mean travel times  $\tau_{\text{mean}}(\mathbf{x}_1 | \mathbf{x}_2) = (\tau_+ + \tau_-)/2$  are mostly sensitive to wave-speed perturbations. In practice, some spatial averaging is often necessary before the fit is performed.

An alternative definition of travel time was introduced by Gizon & Birch (2002, 2004) by analogy with a definition used in Earth seismology (Zhao & Jordan, 1998). This method was designed to obtain travel times from cross-covariances measured with short  $T$  and with as little spatial averaging as possible. By definition, the travel times  $\tau_+$  and  $\tau_-$  are given by

$$\tau_{\pm}(\mathbf{x}_1 | \mathbf{x}_2) = \int w_{\pm}(\mathbf{x}_2 - \mathbf{x}_1, t) [C(\mathbf{x}_1 | \mathbf{x}_2, t) - C_0(\mathbf{x}_2 - \mathbf{x}_1, t)] dt, \quad (7)$$

where the weight functions are

$$w_{\pm}(\Delta, t) = \mp \frac{f(\pm t) \partial_t C_0(\Delta, t)}{\int dt' f(\pm t') [\partial_{t'} C_0(\Delta, t')]^2}. \quad (8)$$

The function  $C^0$  is a smooth reference cross-correlation derived from a horizontally homogeneous solar model. The function  $f(t)$  is a one-sided function (zero for  $t < 0$ ) used to separately measure the travel times from the positive- and negative-time parts of the cross-covariance function. A standard choice is a function  $f$  that targets the first-skip branch of the cross-covariance function. In the following, we use this second definition (Eq. [7]) of travel times.

## 3. RING PARAMETERS

In ring diagram analysis, a local power spectrum is analyzed at constant values of the wavenumber. At fixed  $k = \|\mathbf{k}\|$ , the power depends on  $\omega$  and the direction of  $\mathbf{k}$  denoted by the angle  $\theta$  measured anticlockwise from the  $+x$  direction. A constant horizontal flow  $\mathbf{u}$  would shift the whole power by an amount  $\Delta\omega = k \cos \theta u_x + k \sin \theta u_y$ . A more general

internal flow, however, will cause a Doppler shift which depends on  $k$  and on the radial order,  $n$ , of the modes of oscillations. Ring diagram analysis consists of extracting, in  $\theta$ - $\omega$  space, a vector parameter  $\mathbf{u}^{(kn)}$  for each value of  $k$  and  $n$ . The inversion of these parameters gives access to the physical flow field (denoted by  $\mathbf{v}$ ) in the upper convection zone.

Here we propose a simple method to extract ring parameters from local power spectra. We only consider flow parameters for the sake of simplicity. This method is motivated, in part, by the need to facilitate the derivation of three-dimensional sensitivity kernels for flows. At constant  $k$ , the joint probability density function of the power in the ridge  $n$  can be approximated by

$$\text{pdf}(P) \simeq \prod_{\omega, \theta} \frac{g_n(\omega)}{\overline{P}(\mathbf{k}, \omega)} \exp[-P(\mathbf{k}, \omega)/\overline{P}(\mathbf{k}, \omega)], \quad (9)$$

where products are over all frequencies  $\omega$  and angles  $\theta$ , the function  $\overline{P}$  is the expectation value of  $P$ , and the window function  $g_n(\omega)$  selects a region in frequency space centered around the ridge with radial order  $n$ . In  $\theta$ - $\omega$  space, the vector  $\mathbf{k} = \hat{\mathbf{x}}k \cos \theta + \hat{\mathbf{y}}k \sin \theta$  is only a function of  $\theta$ . Equation (9) assumes that data points are uncorrelated in  $\theta$ - $\omega$  space; this is a useful first approximation. Let us denote by  $P_0(\mathbf{k}, \omega)$  a known reference power spectrum which does not depend on the direction of  $\mathbf{k}$  and which is a good approximation to the expectation value of the observed local power spectrum. The model that we want to fit to the data is

$$\overline{P}(\mathbf{k}, \omega) = P_0(k, \omega) - \mathbf{k} \cdot \mathbf{u}^{(kn)} \partial_\omega P_0(k, \omega) + \dots \quad (10)$$

This linearization is valid when the flow velocity is smaller than the phase velocity of the waves. The vector  $\mathbf{u}^{(kn)}$  that provides the best fit to the data is obtained by maximizing the log-likelihood,  $\ln(\text{pdf})$ . To first order, we obtain

$$\int_0^{2\pi} d\theta \int d\omega g_n(\omega) P_0^{-2} (P - P_0 + \mathbf{k} \cdot \mathbf{u}^{(kn)} \partial_\omega P_0) \mathbf{k} \partial_\omega P_0 = 0. \quad (11)$$

Using  $\int_0^{2\pi} d\theta (\mathbf{k} \cdot \mathbf{u}) \mathbf{k} = \pi k^2 \mathbf{u}$ , we find that

$$\mathbf{u}^{(kn)}(\mathbf{x}) = \int_0^{2\pi} d\theta \int d\omega \mathbf{W}^{(kn)}(\theta, \omega) [P(\mathbf{k}, \omega; \mathbf{x}) - P_0(k, \omega)], \quad (12)$$

where the two-dimensional vector  $\mathbf{W}^{(kn)}$  is defined by

$$\mathbf{W}^{(kn)}(\theta, \omega) = - \frac{(\hat{\mathbf{x}}k \cos \theta + \hat{\mathbf{y}}k \sin \theta) g_n(\omega) [P_0(k, \omega)]^{-2} \partial_\omega P_0(k, \omega)}{\pi k^2 \int d\omega' g_n(\omega') [P_0(k, \omega')]^{-2} [\partial_\omega P_0(k, \omega')]^2}. \quad (13)$$

The aim of the above discussion was to provide some motivation for equations (12) and (13). From now on, however, we elect equation (12) as a definition for the ring parameters  $\mathbf{u}^{(kn)}(\mathbf{x})$ .

#### 4. NOISE

The main source of noise in local helioseismology is due to the stochastic nature of solar oscillations. A good understanding of the properties of noise is useful for a correct interpretation of the measurements and, in particular, for solving the inverse problem. In time-distance helioseismology, noise information is given by the noise covariance matrix of the travel times:

$$\Lambda_{\text{td}} = \text{Cov}[\tau_{a,i}(\mathbf{x}_1, \mathbf{x}_2), \tau_{b,j}(\mathbf{x}'_1, \mathbf{x}'_2)], \quad (14)$$

where indices  $a$  and  $b$  refer to different types of travel times (+, -, mean, diff) and indices  $i$  and  $j$  refer to various types of weight functions  $W_i$  and  $W_j$ , which may differ as a result of different Fourier filters,  $F_i$  and  $F_j$  (see Eq. [2]).

Similarly, in ring-diagram analysis, the noise covariance matrix between measurements is

$$\Lambda_{\text{rd}} = \text{Cov}[u_i^{(kn)}(\mathbf{x}), u_j^{(k'n')}(\mathbf{x}')], \quad (15)$$

where indices  $i$  and  $j$  correspond to either the  $x$  or the  $y$  component of  $\mathbf{u}$ .

So far, noise has been studied for the quiet Sun under the assumption that the medium is horizontally homogeneous. The noise covariance matrices can be estimated directly by averaging over many samples of the data, as was done by Jensen et al. (2003) in the case of time-distance helioseismology. It is also possible to obtain an accurate estimate of the

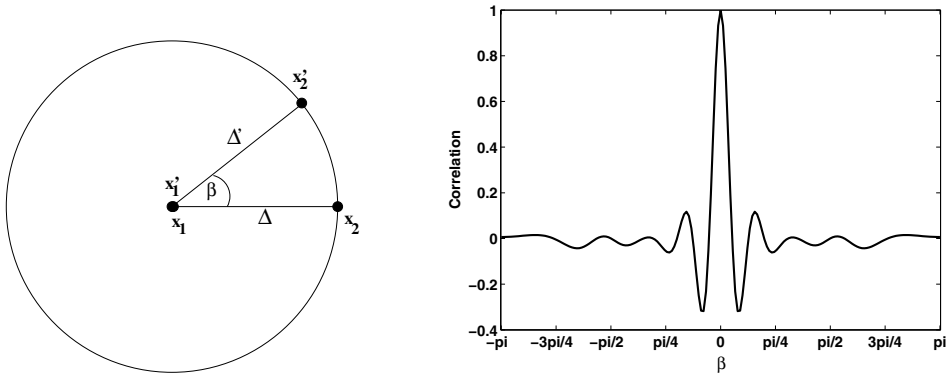


Figure 1. Noise correlation between  $f$ -mode travel times  $\tau_{\text{diff}}(\mathbf{x}_1|\mathbf{x}_2)$  and  $\tau_{\text{diff}}(\mathbf{x}'_1|\mathbf{x}'_2)$  in the case  $\mathbf{x}_1 = \mathbf{x}'_1$  and  $\Delta = \Delta' = 10$  Mm. The left panel describes the geometry, the right panel shows the correlation as a function of the angle  $\beta$ .

noise covariance from a statistical model of the oscillation signal (Gizon & Birch, 2004). In general, the noise covariance matrices given by equations (14) and (15) depend on the fourth moments of the wavefield,

$$\text{Cov}[\phi^*(\mathbf{k}_1, \omega_1)\phi(\mathbf{k}_2, \omega_2), \phi^*(\mathbf{k}_3, \omega_3)\phi(\mathbf{k}_4, \omega_4)], \quad (16)$$

which can be written down explicitly when the  $\phi(\mathbf{k}, \omega)$  are assumed to be uncorrelated on the Fourier grid and normally distributed. These moments can be used for computing the noise correlation matrix for both time-distance and ring-diagram measurements.

One particular example is given in Figure 1. In this example, we have modeled the correlation between two  $f$ -mode travel times  $\tau_{\text{diff}}(\mathbf{x}_1|\mathbf{x}_2)$  and  $\tau_{\text{diff}}(\mathbf{x}'_1|\mathbf{x}'_2)$  in the case  $\mathbf{x}_1 = \mathbf{x}'_1$  and  $\|\mathbf{x}_2 - \mathbf{x}_1\| = \|\mathbf{x}'_2 - \mathbf{x}'_1\| = 10$  Mm. One sees how the correlation drops and oscillates as the angle between the two pairs of points,  $\beta$ , increases. This type of information is needed to compute optimally localized averages of the kernels for the inversion of time-distance data. It may also be useful to improve the standard averaging of the travel times over quadrants (Duvall et al., 1997).

## 5. WAVEFIELD PERTURBATION IN THE BORN APPROXIMATION

Given a smooth reference solar model, the linear forward problem of local helioseismology is to compute the perturbations in travel times and ring parameters caused by small amplitude inhomogeneities superimposed on the reference solar model.

The equations of adiabatic oscillations may be written in the form

$$L[\xi] \equiv -\bar{\rho} \frac{D^2 \xi}{Dt^2} + \nabla(\Gamma_1 \bar{p} \nabla \cdot \xi + \xi \cdot \nabla \bar{p}) - (\nabla \cdot \xi) \nabla \bar{p} - \xi \cdot \nabla(\nabla \bar{p}) + \Upsilon[\xi] = \mathbf{S}, \quad (17)$$

where  $\Gamma_1$ ,  $\bar{\rho}$ , and  $\bar{p}$  are the first adiabatic exponent, density, and pressure in the background state. The operator  $D/Dt = \partial/\partial t + \mathbf{v} \cdot \nabla$  is the material derivative,  $\Upsilon$  is a phenomenological damping operator, and  $\mathbf{S}$  is a stochastic source function (granulation). In Sections 6 and 7, we focus on the effect of the flow  $\mathbf{v}(\mathbf{r})$  on oscillations.

In the absence of a flow, we label all quantities with the superscript 0, so that  $L^0[\xi^0] = \mathbf{S}^0$ . The zero-order source function,  $\mathbf{S}^0$ , is assumed to be horizontally homogeneous and stationary in time. For a background model where density and pressure only depend on height,  $z$ , the solution to this problem (Birch et al., 2004) can be written in terms of the Green's tensor,  $G_j^i$ , given by

$$L^0[\mathbf{G}^i(\mathbf{r}|\mathbf{r}', t|t')] = \hat{\mathbf{e}}_i \delta(\mathbf{r} - \mathbf{r}') \delta(t - t'), \quad (18)$$

where  $\hat{\mathbf{e}}_i$  is a unit vector in the direction of the  $i$ -th spatial coordinate. The symmetry of the zero-order Green's tensor is such that  $G_j^i(\mathbf{r}|\mathbf{r}', t|t') = G_j^i(\mathbf{x} - \mathbf{x}', t - t', z|z')$  with  $\mathbf{r} = (\mathbf{x}, z)$  and  $\mathbf{r}' = (\mathbf{x}', z')$ . Under the assumption that the sources of excitation are located at a particular height  $z_s$ , and using equation (1), the line-of-sight component of the wave velocity can be written in Fourier space as

$$\phi^0(\mathbf{k}, \omega) = (2\pi)^3 \mathcal{G}^i(\mathbf{k}, \omega, z|z_s) S_i^0(\mathbf{k}, \omega; z_s) \quad (19)$$

where  $\mathcal{G}^i(\mathbf{k}, \omega) = -i\omega \text{MTF}(\mathbf{k}) \ell_j G_j^i(\mathbf{k}, \omega)$  is the Green's function for the observable and the MTF is the spatial transform of the PSF. We use the same conventions for the Fourier transforms as in Gizon & Birch (2002) and sums over repeated indices are implicit.

When the flow,  $\mathbf{v}$ , is switched on, the first order perturbation to the wave displacement satisfies

$$L^0[\delta\xi] = -\delta L[\xi^0] + \delta S = 2\bar{\rho}\mathbf{v} \cdot \nabla \partial_t \xi^0 - \delta\Upsilon[\xi^0] + \delta S. \quad (20)$$

For any function  $f$ , the change  $\delta f = f - f^0$  is measured with respect to its zero-order value. In the above equation (Eq. [20]), we have included the perturbations to the damping operator and to the source function. These two terms should not be neglected *a priori*. Physically, the perturbation to the source function can be understood as the advection of the granulation by the flow, causing a Doppler shift. An estimate of  $\delta S$  and  $\delta\Upsilon$  can be obtained by performing a Galilean transformation to a frame in which the fluid is locally at rest: in the space-frequency domain  $\delta f(\mathbf{r}, \omega) = i\mathbf{v}(\mathbf{r}) \cdot \nabla_{\mathbf{r}} \partial_\omega f^0$  is approximately true in the neighborhood of  $\mathbf{r}$ . Based on an analysis of the f-mode travel-time kernels shown in Section 6, we find that the term  $\delta\Upsilon \phi^0$  is typically one order of magnitude smaller than  $\delta L[\xi^0]$ , while  $\delta S$  is even smaller. Thus, the perturbed wavefield is approximately given by

$$\delta\phi(\mathbf{k}, \omega) \simeq -2i\omega(2\pi)^4 \int d^3\mathbf{r} d^2\mathbf{k}' \mathcal{G}^j(\mathbf{k}, \omega, z_0|z) e^{-i\mathbf{k}\cdot\mathbf{x}} \bar{\rho}(z)\mathbf{v}(\mathbf{r}) \cdot \nabla_{\mathbf{r}} [G_j^i(\mathbf{k}', \omega, z, z_s) e^{i\mathbf{k}'\cdot\mathbf{x}}] S_i(\mathbf{k}', \omega; z_s) \quad (21)$$

The accuracy of the Born approximation has been studied by Birch & Felder (2004) by comparison with numerical simulations of acoustic wave propagation through simple flows in two dimensions. The numerical experiments show that the Born approximation captures the basic behavior of the travel times. Later in Section 8 we test the accuracy of the Born approximation for magnetic perturbations.

## 6. SENSITIVITY OF F-MODE TRAVEL TIMES TO FLOWS

The sensitivity of travel times to local perturbations in internal solar properties can be described through linear sensitivity functions, also called travel-time kernels. Gizon & Birch (2002) gave a general recipe for computing such travel-time kernels using the Born approximation. Birch et al. (2004) calculated kernel functions for the case of sound-speed perturbations. Gizon & Birch (2002) applied the same procedure to obtain approximate kernels for the two-dimensional sensitivity of f-mode travel times to near-surface perturbations (non-uniform source strength and wave damping perturbations). Here we extend their method and apply it to the specific case of flows.

We consider the interaction of waves at the interface of an infinitely deep, constant density medium with a steady flow. It can be shown that if the flow,  $\mathbf{v}$ , is irrotational then the first-order perturbation to the velocity potential can be written as a surface integral that involves the unperturbed velocity potential and the horizontal flow at the surface. We find that the first-order perturbation to the cross-correlation,

$$\delta C(\mathbf{x}_1|\mathbf{x}_2, \omega) = \frac{2\pi}{T} E[\delta\psi^*(\mathbf{x}_1, \omega)\psi(\mathbf{x}_2, \omega) + \psi^*(\mathbf{x}_1, \omega)\delta\psi(\mathbf{x}_2, \omega)], \quad (22)$$

is of the form

$$\delta C(\mathbf{x}_1|\mathbf{x}_2, \omega) = \int_{\partial\odot} \mathbf{C}(\mathbf{x}_1|\mathbf{x}_2, \omega; \mathbf{r}) \cdot \mathbf{v}(\mathbf{r}) d^2\mathbf{r}, \quad (23)$$

where the vector  $\mathbf{C}$  is horizontal and does not depend on  $\mathbf{v}$ . The travel-time definition (Eq. [7]) implies that the perturbation in the travel-time difference,  $\tau_{\text{diff}} = \tau_+ - \tau_-$ , becomes

$$\delta\tau_{\text{diff}}(\mathbf{x}_1|\mathbf{x}_2) = \int_{\partial\odot} \mathbf{K}(\mathbf{x}_1|\mathbf{x}_2; \mathbf{r}) \cdot \mathbf{v}(\mathbf{r}) d^2\mathbf{r}, \quad (24)$$

where the vector sensitivity kernel to a horizontal flow is

$$\mathbf{K}(\mathbf{x}_1|\mathbf{x}_2, \mathbf{r}) = 4\pi \text{Re} \int_0^\infty w_{\text{diff}}^*(\mathbf{x}_1|\mathbf{x}_2, \omega) \mathbf{C}(\mathbf{x}_1|\mathbf{x}_2, \omega; \mathbf{r}) d\omega. \quad (25)$$

The weight function  $w_{\text{diff}} = w_+ - w_-$  depends on the zero-order cross-correlation function (Eq. [8]). We note that implicit in the definition of the kernels are the effects of the line of sight projection of the velocity field (see Eq. [1]), although for what follows we report only the case  $\ell = \hat{\mathbf{z}}$ . Furthermore, we included the effects of  $\delta S$  and  $\delta\Upsilon$  in the calculation, which were found to be small. A typical example of kernel functions is given in Figure 2.

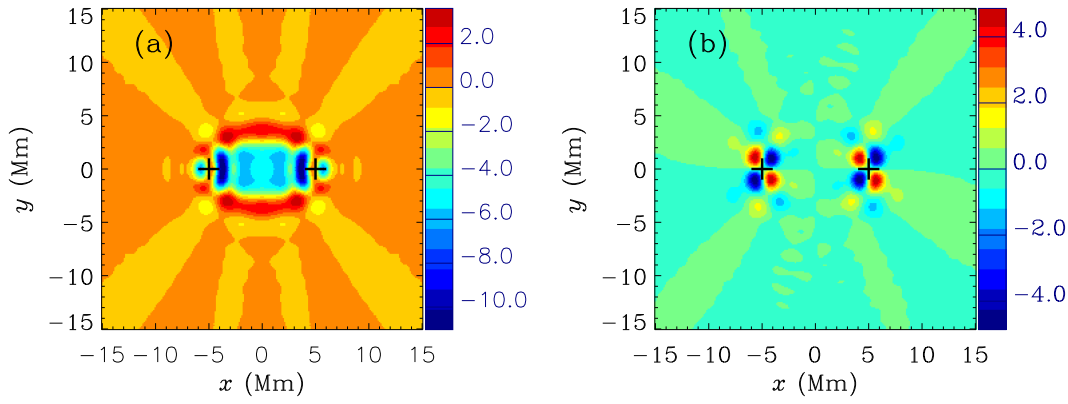


Figure 2. Two-dimensional  $f$ -mode sensitivity kernels for flows. The observation points (crosses) have coordinates  $\mathbf{x}_1 = (-5, 0)$  Mm and  $\mathbf{x}_2 = (5, 0)$  Mm. (a) Kernel  $K_x$  which gives the sensitivity to the  $x$ -component of flow,  $v_x$ . (b) Kernel  $K_y$ . The color bars are in units of  $\text{s (km/s)}^{-1} \text{Mm}^{-2}$ . Note the change of scale in the color map between the two figures. The numerical calculation of one kernel takes about one hour on a Sun workstation. The total integral of  $K_x$  is  $-196 \text{ s (km/s)}^{-1}$  and the integral of  $K_y$  is zero.

## 7. THREE-DIMENSIONAL FLOW KERNELS FOR RING-DIAGRAM ANALYSIS

Until now, only one-dimensional kernels have been computed for the ring-diagram analysis of flows (e.g. Basu et al., 1999). In order to obtain the three-dimensional sensitivity kernels for the ring parameters  $\mathbf{u}^{(kn)}$ , we must compute the first-order perturbation to the local power spectrum,

$$\delta P(\mathbf{k}, \omega; \mathbf{x}) = 2\text{Re} \int d\mathbf{k}_1 d\mathbf{k}_2 A(\mathbf{k} - \mathbf{k}_1; \mathbf{x}) A^*(\mathbf{k} - \mathbf{k}_2; \mathbf{x}) E [\delta\phi(\mathbf{k}_1, \omega) \phi^{0*}(\mathbf{k}_2, \omega)]. \quad (26)$$

Using equation (21), we find that  $\delta P$  can be written in the form

$$\delta P(\mathbf{k}, \omega; \mathbf{x}) = \int_{\odot} \mathbf{\Pi}(\mathbf{k}, \omega; \mathbf{r}) \cdot \mathbf{v}(\mathbf{r}) d^3\mathbf{r}, \quad (27)$$

where the three-dimensional vector  $\mathbf{\Pi}$  gives the local sensitivity of  $\delta P$  to a flow  $\mathbf{v}$ . Then, using the linearized fitting procedure (Eq. [12]) with  $P - P_0 = \delta P$ , we obtain

$$\mathbf{u}^{(kn)}(\mathbf{x}) = \int_{\odot} \mathbf{K}_j^{(kn)}(\mathbf{r}) v_j(\mathbf{r}) d^3\mathbf{r}, \quad (28)$$

where the kernel vectors are given by

$$\mathbf{K}_j^{(kn)}(\mathbf{r}) = \int_0^{2\pi} d\theta \int d\omega \mathbf{W}^{(kn)}(\theta, \omega) \Pi_j(\mathbf{k}, \omega; \mathbf{r}). \quad (29)$$

We have computed ring kernels using a normal-mode summation for the Green's function (Birch et al., 2004). Figure 3 shows a  $y = 0$  cut through  $K_x^{(kn)}(\mathbf{r})$  for  $k = 300/R_{\odot}$  and  $n = 4$ . These ring-diagram kernels promise to be useful for the three-dimensional inversion of dense-pack (overlapping tiles) ring parameters. It is reassuring to see that the depth dependence of these kernels (Fig. 3, right panel) is not too different from that of the one-dimensional kernels (which scale like the kinetic energy density; see Basu et al., 1999).

## 8. EFFECT OF A WEAK MAGNETIC FIELD

Can the magnetic field be measured in the solar interior? A major goal of helioseismology is to detect and image the magnetic field,  $\mathbf{B}$ , in the solar interior. This has not been accomplished yet. Observations have shown that the frequencies, phases, and amplitudes of solar oscillations are perturbed in regions of enhanced magnetic activity. Knowing the frequencies of the global modes of oscillations, however, is not sufficient to disentangle weak magnetic perturbations from

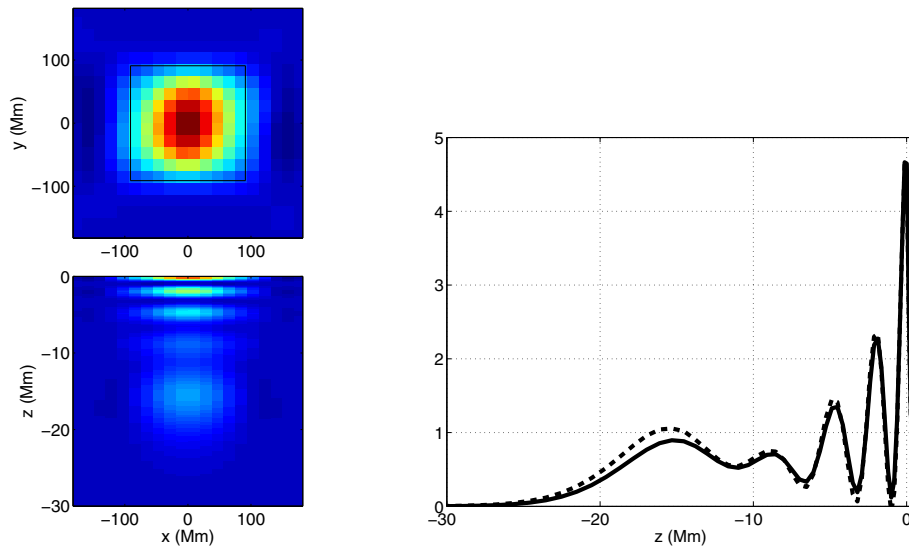


Figure 3. Left: Slices  $z = 0$  (top) and  $y = 0$  (bottom) through the ring kernel  $K_x^{(kn)}(\mathbf{r})$  for  $k = 300/R_\odot$  and  $n = 4$ . Right: Plot of  $K_x^{(kn)}$  at fixed  $x = y = 0$  as a function of height (dashed) and a curve proportional to the kinetic energy density  $\rho \|\xi\|^2$  for comparison (solid).

other aspherical perturbations (Zweibel & Gough, 1995); global-mode frequencies can only provide an upper limit for the strength of a buried magnetic field (e.g. Basu, 1997). The specific signature of  $\mathbf{B}$  resides in the anisotropic distortion to the eigenfunctions. For this reason, it is necessary to turn to methods of local helioseismology to search for the signature of the magnetic field.

As discussed by e.g. Cally (2005) the interaction of acoustic waves with sunspot magnetic fields is strong in the near surface layers. As a result, the effect of the magnetic field on the travel times is not expected to be small near the surface. Deeper inside the Sun, however, the ratio of the magnetic pressure to the gas pressure becomes small, and it is tempting to treat the effects of the magnetic field on the waves using perturbation theory. The hope is to eventually develop a linear inversion to estimate the subsurface magnetic field from travel times measured between surface locations that are free of magnetic field. Of particular interest is the search for a magnetic field at the bottom of the convection zone.

With the aim of studying magnetic effects in time-distance helioseismology, we used the first-order Born approximation to compute the scattering of small amplitude acoustic plane waves by a magnetic cylinder embedded in an otherwise uniform medium (Gizon et al., 2006). Because this simple problem has a known exact solution for arbitrary magnetic field strengths (Wilson, 1980), we can study the validity of the linearization of the wavefield on the square of the magnetic field. The validity of the Born approximation is not a priori obvious since the magnetic field allows additional wave modes.

We used the ideal equations of ideal magnetohydrodynamics, the ideal gas equation of state, and a simple energy equation which neglects all forms of heat losses. We considered a magnetic cylinder with radius  $R$  and uniform magnetic field strength  $B$  embedded in an infinite, otherwise uniform, gravity free medium with constant density  $\rho_0$ , gas pressure  $p_0$ , and temperature  $T_0$ . We chose to study the case where the background temperature is the same inside and outside the magnetized region; thus the sound speed,  $c$ , is constant everywhere. This choice was motivated by our desire to restrict ourselves, as much as possible, to the study of the effect of the Lorentz force on waves, rather than the effect of a sound speed variation. We considered a plane wave incident on the magnetic tube, with pressure fluctuations of the form

$$p_{\text{inc}}(\mathbf{x}, z, t) = P \exp(i\mathbf{k}_\omega \cdot \mathbf{x} + ik_z z - i\omega t), \quad (30)$$

where  $P$  is an amplitude,  $\mathbf{x}$  is a position vector perpendicular to the cylinder axis, and  $z$  is the coordinate along the cylinder axis. The vector  $\mathbf{k}_\omega$  is the component of the wave vector perpendicular to the tube axis with magnitude  $k_\omega = \sqrt{\omega^2/c^2 - k_z^2}$ .

We solved the above problem exactly and in the Born approximation. The exact solution, found by Wilson (1980), is such that the total wave pressure, hydrodynamic plus magnetic, and the radial velocity must be continuous across the tube boundary. This exact solution is valid for arbitrarily large values of  $B$  and  $R$ . For the Born approximation, we included

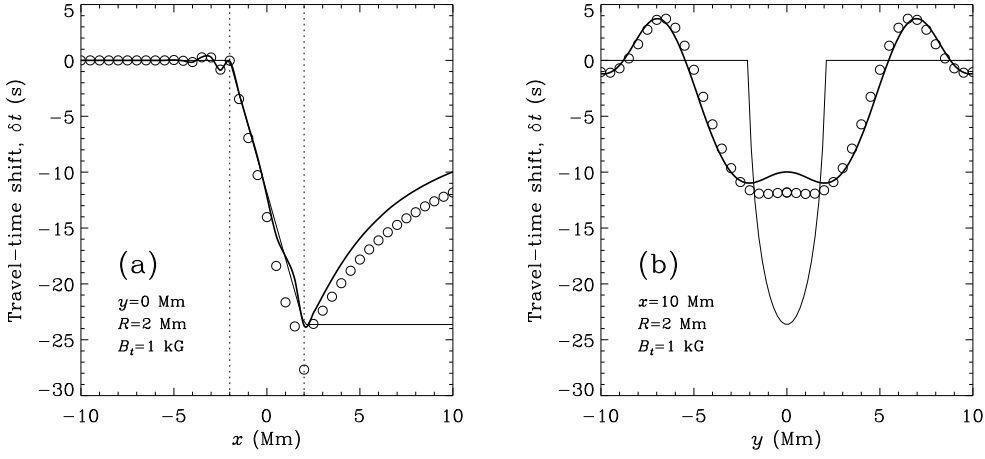


Figure 4. Local travel-time shifts  $\delta t(\mathbf{x})$  caused by a magnetic cylinder with  $\epsilon = 0.13$ . The travel times are measured at positions  $\mathbf{x} = (x, y)$  in a plane perpendicular to the cylinder axis. The incoming acoustic wavepacket moves in the  $+x$  direction. The radius of the tube is  $R = 2$  Mm and the tube axis is at  $(x, y) = (0, 0)$ . In both panels the heavy solid line is for the exact travel-time shift, the circles are for the Born approximation, and the thin line is for the ray approximation. The left panel shows the travel-time shifts as a function of  $x$  at fixed  $y = 0$ . The right panel shows the travel-time shifts as a function of  $y$  at fixed  $x = 10$  Mm.

both the magnetic perturbations to the steady background state and to the wavefield. Since the Lorentz force is quadratic in the magnetic field, we introduced a small parameter,

$$\epsilon = \frac{B^2}{4\pi\rho_0 c^2}, \quad (31)$$

that is second order in the magnetic field. Retaining the terms of order  $\epsilon$  we find that the equations for the scattered pressure field,  $p_{sc}$ , reduce to a forced Helmholtz equation.

The main result of this investigation (Gizon et al., 2006), which cannot be discussed here in full detail, is that the exact solution and the Born solution are identical to first order in  $\epsilon$ , inside and outside the magnetic cylinder.

We have also compared seismic travel-time shifts computed in the Born approximation and from the exact solution. For the sake of simplicity, we fix  $k_z = 0$ . Using Cartesian coordinates  $\mathbf{x} = (x, y)$  for the horizontal plane, we choose an incoming Gaussian wavepacket propagating in the  $+x$  horizontal direction:

$$p_{inc}(\mathbf{x}, z, t) = \int_0^\infty e^{-(\omega - \omega_*)^2 / (2\sigma^2)} \cos[\omega(x/c - t)] d\omega. \quad (32)$$

where  $\omega_*/2\pi = 3$  mHz is the dominant frequency of solar oscillations and  $\sigma/2\pi = 1$  mHz is the dispersion. The wavepacket is centered on the magnetic tube at time  $t = 0$ . The parameters of the steady background at infinity are  $\rho_0 = 5 \times 10^{-7}$  cgs and  $c = 11$  km/s, which are roughly the conditions at a depth of 250 km below the solar photosphere. By definition, the travel-time shift caused by the magnetic tube at location  $\mathbf{x}$  is the time  $\delta t(\mathbf{x})$  that minimizes the function

$$X(t) = \int [p_{tot}(\mathbf{x}, t') - p_{inc}(\mathbf{x}, t' - t)]^2 dt', \quad (33)$$

where  $p_{tot}$  is the full wavefield that includes both the incident wavepacket and the scattered wave packet caused by the magnetic field. The travel-time shifts can be computed in this way for either the exact solution or the Born-approximation for  $p_{tot}$ .

Figure 4 shows travel-time shifts resulting from a flux tube of radius 2 Mm and field strength  $B = 1$  kG ( $\epsilon = 0.13$ ). Figure 4a shows the exact, Born-, and ray-approximation travel times as a function of  $x$  at fixed  $y$ . Ray approximation travel-time shifts are given by equation (14) from Kosovichev & Duvall (1997). Inside the flux tube, the Born-approximation travel times reproduce the exact travel times at a good level of accuracy (the error is of order  $\epsilon$ ). As  $x$  increases to the right of the tube, wavefront healing (e.g. Nolet & Dahlen, 2000) is seen in the exact and Born approximation travel times. Wavefront healing, however, is not seen in the ray approximation travel times. Figure 4b shows the travel times as a

function of  $y$  at fixed  $x = 10$  Mm. The Born approximation reproduces the exact travel times to within 20%. The ray approximation does not capture finite wavelength effects and does not capture the basic behavior of the travel times; it can be inaccurate by many orders of magnitude for  $kR \ll 1$ .

We conclude that, for typical values of the solar magnetic field, the Born approximation should be good at depths larger than a few hundred km below the photosphere. The condition  $\epsilon \ll 1$  is satisfied for a 1-kG magnetic fibril at a depth of 250 km ( $\epsilon \approx 0.1$ ) and for a  $10^5$  G magnetic flux tube at the base of the convection zone ( $\epsilon \approx 10^{-7}$ ). The present work suggests that travel-time kernels for the subsurface magnetic field will be useful for probing depths greater than a few hundred km beneath the photosphere, at least in the case when the travel times are measured between surface points that are not in magnetic regions. We have not addressed, however, the important question of how to separate unambiguously magnetic perturbations from other perturbations that also affect wave travel times, e.g. temperature and density inhomogeneities.

Near the photosphere,  $\epsilon$  is not small. It has been suggested by many authors (e.g. Lindsey & Braun, 2004) that in this case the Born approximation will fail. An exception is the claim by Rosenthal (1995) that the Born approximation will remain valid for kG magnetic fibrils in the limit as the ratio of the radius of the magnetic element to the wavelength goes to zero. Using our simple problem, we found that, for arbitrary magnetic field strength, the Born approximation is not valid in the limit of small tube radius.

## 9. OBSERVATION OF TRAVEL-TIME SHIFTS DUE TO LOCALIZED MAGNETIC FEATURES

As we have seen for example in Section 6, time-distance helioseismology critically relies on models of the sensitivity of seismic travel times to localized heterogeneities. Yet, the 'banana-doughnut' kernels used in finite-wavelength tomography of the Earth (Dahlen et al., 2000) or the Sun (Birch & Kosovichev, 2000) have been received with some skepticism (e.g. de Hoop et al., 2005). These kernels have to be trusted on the ground that they work for simple test cases (such as the one in Sec. 8). Here we use time-distance helioseismology to directly measure the spatial sensitivity of f-mode travel times to a point-like magnetic perturbation. The data strongly speak in favour of 'banana-doughnut' theory according to which body-wave travel times are sensitive to the wave speed in a broad region surrounding the geometrical ray path.

The solar surface magnetic field is dragged by convective motions into concentrations that form the quiet-Sun magnetic network. Because these magnetic features are smaller than the wavelengths of solar oscillations, they are ideal to study the response of finite-wavelength seismic travel times to point-like perturbations. We used f modes with a dominant wavelength of 5 Mm. These waves propagate horizontally in the top 2 Mm beneath the solar surface.

We used 400 hours of high-resolution MDI images of the line-of-sight magnetic field and of the line-of-sight velocity obtained in 1996-97 (Scherrer et al., 1995). We measured the positions of the most localised magnetic features in each 4-hour interval. On average, these features have a width of 2.6 Mm. The velocity images were used for seismic analysis. For each 4-hour interval, we use the measurement technique described in Section 2 to measure f-mode travel times between any two locations separated by a fixed distance of 9.9 Mm. In order to reduce random noise, the travel-time maps were shifted, de-rotated, and averaged over all the magnetic features to obtain a map of the travel-time sensitivity to a local magnetic perturbation. Figure 5a reveals that the sensitivity is not restricted to the geometrical ray path, is spread on an ellipse, and oscillatory.

We developed a simple phenomenological model to explain the basic features of the travel-time observations. Motivated by studies of slender magnetic tubes (Bogdan et al., 1996), we assumed that scattering from a magnetic feature can be described by a combination of monopole and dipole scattering. Treating solar surface waves as deep water waves (Gizon & Birch, 2002), we computed the wave field using a single-scattering approximation, and then adjusted the complex scattering amplitudes to obtain the best match with the observations. We find that the dipole and monopole contributions are equally important. Figure 5b shows that this model is able to reproduce the main features of the observations. The ellipse and hyperbola shaped features are of roughly the same amplitude and in the same locations. It is likely that in-depth physical modelling would yield information about the detailed structure of small magnetic features in the solar atmosphere.

By studying the interaction of seismic waves with localised magnetic features on the Sun, we have provided an observational confirmation of the basic banana-doughnut theory originally developed for finite-wavelength tomography of the Earth. This is the first test outside the laboratory showing the relevance of scattering theory to cross-correlation travel times (laboratory tests exist for ultrasonic waves, see Spetzler et al., 2002). As in Earth seismology, we suggest that finite-wavelength modelling will be essential in revealing deep structures in the solar interior.

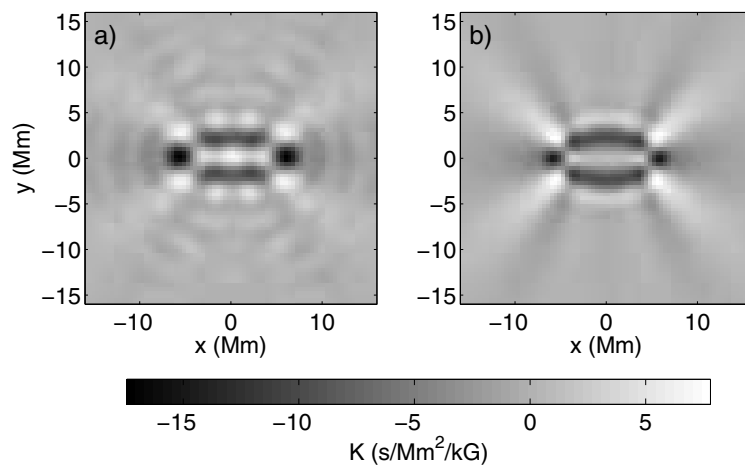


Figure 5. Sensitivity of solar surface-wave travel times to small magnetic features. (a) Observations based on MDI data from the high-resolution field of view. A magnetic feature at position  $(x, y)$  causes a shift in the travel time measured between the two observation points (at  $x = \pm 4.95$  Mm,  $y = 0$ ). As magnetic features have a finite spatial extent, we applied a simple regularized deconvolution. The grey scale gives the shift in travel time due to a 1 kG magnetic field covering 1 Mm<sup>2</sup>. (b) Phenomenological model for a point magnetic scatterer based on single-scattering theory. A scatterer located anywhere along an ellipse (with foci at the observation points) causes travel-time shifts of the same sign, giving rise to Fresnel zones. The hyperbolic features are due to the scattering of waves generated by distant sources.

## REFERENCES

- Basu S., 1997, MNRAS 288, 572  
 Basu S., Antia H.M., Tripathy S.C., 1999, ApJ 512, 458  
 Birch A.C., Felder G., 2004, ApJ 616, 1261  
 Birch A.C., Kosovichev A.G., 2000, Solar Phys. 192, 193  
 Birch A.C., Kosovichev A.G., Duvall T.L. Jr., 2004, ApJ 608, 580  
 Bogdan T.J., Hindman B.W., Cally P.S., 1996, ApJ 465, 406  
 Cally P.S., 2005, MNRAS 358, 353  
 Dahlen F.A., Hung S.-H., Nolet G., 2000, Geophys. J. Int. 160, 621  
 de Hoop M., van der Hilst R., 2005, Geophys. J. Int. 160, 621  
 Duvall T.L. Jr., Kosovichev A.G., Scherrer P.H. et al., 1997, Solar Phys. 170, 63  
 Gizon L., Birch A.C., 2002, ApJ 571, 966  
 Gizon L., Birch A.C., 2004, ApJ 614, 472  
 Gizon L., Birch A.C., 2005, Living Rev. Solar Phys. 2, 6  
 Gizon L., Hanasoge S., Birch A.C., 2006, ApJ, submitted  
 Haber D.A., Hindman B.W., Toomre J., Thompson M.J., 2004, Solar Phys. 220, 371  
 Jensen J.M., Duvall T.L. Jr., Jacobsen B., 2003, in Local and Global Helioseismology: The Present and Future, ESA SP-517, 315  
 Kosovichev A.G., Duvall T.L. Jr., 1997, in Solar Convection and Oscillations and their Relationship, ASSL Vol. 22, 241  
 Lindsey C., Braun D.C., 2004, ApJS 155, 209  
 Montelli R., Nolet G., Dahlen F.A., Masters G., Engdahl E.R., Hung S.-H., 2004, Science 303, 338  
 Nolet G., Dahlen F.A., 2000, J. Geophys. Res. 105, 19043  
 Rosenthal C.S. 1995, ApJ 438, 434  
 Scherrer P.H., Bogart R.S., Bush R.I. et al., 1995, Solar Phys. 162, 129  
 Spetzler J., Sivaji C., Nishizawa O., Fukushima Y., 2002, Geophys. J. Int. 148, 165  
 Wilson P.R., 1980, ApJ 237, 1008  
 Zhao L., Jordan T.H., 1998, Geophys. J. Int. 133, 683  
 Zweibel E.G., Gough D.O., 1995, in Proceedings of the 4th Soho Workshop, ESA SP-376, Vol. 2, 73